Relationship between CME velocity and active region magnetic energy

P. Venkatakrishnan

Udaipur Solar Observatory, Physical Research Laboratory, Udaipur, Rajasthan, India

B. Ravindra

Udaipur Solar Observatory, Physical Research Laboratory, Udaipur, Rajasthan, India

[1] We find an empirical relationship between the initial speed of Coronal Mass Ejection (CME) and the potential magnetic field energy of the associated active region (AR) that closely resembles the Sedov relation between the speed of a blast wave and the blast energy. We conclude that it is the magnetic energy of an AR that drives the CME. The restructuring of the AR field lines in the corona which can push material with Alfven speed and thus inject energy into the plasma on a time scale shorter than the dynamical time of the corona, is a likely process that can drive the CME. The empirical relationship allows the prediction of the maximum speed of a CME that can result from an AR of a given magnetic energy. *INDEX TERMS:* 7513 Solar Physics, Astrophysics, and Astronomy: Coronal mass ejections; 7519 Solar Physics, Astrophysics, and Astronomy: Flares; 7524 Solar Physics, Astrophysics, and Astronomy: Magnetic fields. **Citation:** Venkatakrishnan, P., and B. Ravindra, Relationship between CME velocity and active region magnetic energy, *Geophys. Res. Lett.*, *30*(23), 2181, doi:10.1029/2003GL018100, 2003.

1. Introduction

[2] One of the major tasks in space weather prediction is the estimation of the severity of geomagnetic storms from the properties of the solar causative agencies of these geomagnetic storms. In a recent paper, *Srivastava and Venkatakrishnan* [2002] showed that the initial speeds of CMEs could well provide a reliable estimate of the storm severity. The next step is to find out what property of the associated active region determines the initial speed of the CME. In what follows, we demonstrate that the CME speeds are related to the magnetic energy of the associated active regions.

[3] A CME produced by an AR near central meridian is directed more or less earthward and can be seen by a coronagraph as a halo CME (visible around the entire occulting disk) if these ejections are massive enough. The CMEs heading both towards and away from earth appear as halos. Improved sensitivity of coronagraphs, larger field of view, and better techniques used in measuring the expansion velocity have improved the prediction of arrival time of CME at earth. Availability of continuous line-of-sight magnetogram data from space, free from seeing, night time interruptions and improved sensitivity in measuring the line-of-sight field (errors are of the order of 20 G) provide a better opportunity for finding the relationship between the

AR magnetic field parameters and velocities of the ejecta. Recently it has become possible to track the CME from its origin using Extreme Ultraviolet Imaging Telescope [EIT: *Delaboudiniere et al.*, 1995] out to $30R_\odot$ using Large Angle Spectroscopic Coronagraph (LASCO) [*Brueckner et al.*, 1995]. In the present study, we examine the relationship between the projected speed of CMEs and the AR magnetic energy by analyzing 37 halo CME events.

2. Data and Analysis

[4] To locate the source region of a CME, we used full disk SOHO/EIT 19.5 nm images as well as images taken in other wavelengths such as 17.1 nm, 28.4 nm, 30.4 nm. EIT provides images with a full view of the corona extending up to $1.5R_\odot$. During a flare or a CME, EIT obtains images of the sun at a cadence of every 15–20 min. In few cases of selected CME events the cadence of EIT imaging is $\approx$ 7 hr. We preferred to work with the EIT images, instead of H_α images because we wanted to examine the changes in the corona above active regions and not the chromospheric dynamics.

[5] To find the total energy in the CME related AR, we used full disk Michelson Doppler Imager [MDI: *Scherrer et al.*, 1995] magnetograms taken at a cadence of 96 min as well as 1 min. We could identify the source region of CME in full disk magnetograms with the help of EIT images. In selecting the magnetograms we have restricted ourselves to the following conditions: (1) halo CME should have occurred on those days. (2) the active region responsible for the CME should be located within 30 degree from the central meridian. (3) there should be magnetograms available during the events which may be at the rate of high cadence or may be at a cadence of 96 min. (4) the projected speed of the halo CME should be available. We used white light images obtained from SOHO/MDI to locate and count the saturated pixels in MDI magnetograms (which may be due to the failure in the on-board algorithm when the lookup table saturates).

[6] In order to determine the magnetic potential energy from the line of sight magnetograms, the MDI data must be corrected for the geometrical distortions and instrumental corrections. These include: (1) geometrical foreshortening arising from the spherical geometry of the sun. By choosing a reference time as the instant at which the active region passed through the central meridian, magnetograms are aligned using differential solar rotation [*Howard et al.*, 1990]. We have employed a sub-pixel interpolation with a pixel size of $1''$ [*Chae et al.*, 2001]. (2) correction for the angle between the magnetic field direction and the

2002 July 15
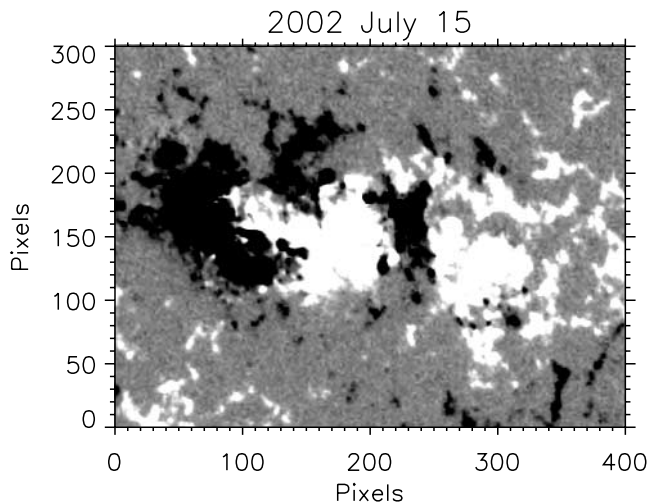
Figure 1. Example of magnetogram which is strong in field strength is shown here. Active region group AR0030 obtained on July 15, 2002.

observer's line of sight. We could correct for the vertical field strength, by multiplying $1/\cos\psi$ to the line-of-sight field strength as in *Chae et al* [2001], where 'ψ' is the heliocentric angle of the region of interest. (3) signal-to-noise ratio is increased by averaging 5 successive 1 min cadence magnetograms. (4) identifying the corrupted pixels in the magnetograms with the help of white light images. Before doing any analysis, we first located the region of saturated pixels. We plotted a scatter plot of intensity vs magnetic field. This plot clearly showed the number of saturated pixels. In our collection of active regions, some of them had saturated pixels. These saturated pixels introduce an error in our potential energy determination of $\approx$4% (upper limit). The potential magnetic field was determined from the observed line-of-sight field using the Fourier method [*Alissandrakis*, 1981]. Using this computed potential field, the potential magnetic energy of the active region was determined by the application of the virial theorem to the photospheric magnetogram [*Chandrasekhar*, 1961; *Molodensky*, 1974; *Low*, 1985]. The actual available or free magnetic energy can only be determined from vector magnetograms which we do not have. We make a reasonable assumption that the free energy is closely related to the potential energy.

[7] The projected speeds of the halo CMEs used in this study are obtained from the on-line SOHO/LASCO CME catalog in which CME kinematics are estimated and compiled from LASCO C2 and C3 images (http://cdaw.gsfc.nasa.gov/cme-list). These CME speeds were determined [*Yashiro et al.*, 2002; *Gopalswamy*, 2003] from linear fits to the height-time plot in the plane-of-sky. The error bars in estimating the speeds are less than 10% [*Yashiro et al.*, 2002].

[8] The source regions of CMEs are determined by EIT images (Fe XII 19.5 nm), using signatures such as coronal dimming and post flare loops. For some of the events the time sequence images of EIT were not available; in those cases we used the LASCO CME mail archive to identify the source regions and Solar Geophysical Data reports to locate the flare regions, which may be associated with CME. In

our collection we have both young as well as decaying ARs. Figure 1 and 2show examples of group of sunspots with strong and weak fields respectively.

[9] To study the relationship between the projected speed of CMEs and the total magnetic energy of the AR, we selected 37 events from 1998 to 2002. In Table 1 we list the selected events, the date and time of occurrence of each CME as observed by C2 coronagraph, the active region which may be responsible for the CME, the location and the projected speed of CME corresponding to those dates and times, estimated total magnetic energy and GOES X-ray flare classes respectively. We plot a graph of $\log_{10}$(projected speed of the ejecta) vs $\log_{10}$(magnetic energy) (Figure 3). The plot shows that there is a fairly strong relationship between the magnetic energy and projected speed. From the plot we could derive the relation between the estimated energy and speed after fitting a linear least square fit curve to the scattered points. The plot gives the relationship between the two as,

$$\log_{10} V = -5.84(\pm 2.69) + 0.26(\pm 0.0822) \log_{10} E$$

where 'E' is the total magnetic energy and 'V' is the projected speed of CME. The terms in the parentheses show the error bars. However, there are several examples in the data where there is a range in the CME speed for a given value of the magnetic energy. This range could well be produced by a range in the fraction of the magnetic energy that actually goes into driving the CME. If this be the case, then one could make an assumption that the uppermost value of the CME speed for a given energy is closer to the maximum possible speed that could be produced for that value of energy. We therefore chose these maximum speeds to plot another straight line (dashes) in Figure 3. We omitted the points beyond $E > 10^{32.9}$ ergs, since the speeds were lower than the speed for $E = 10^{32.9}$ ergs, thereby indicating that only a portion of the magnetic energy might have been utilized for such slower CMEs. Clearly, this is right now

2000 December 18
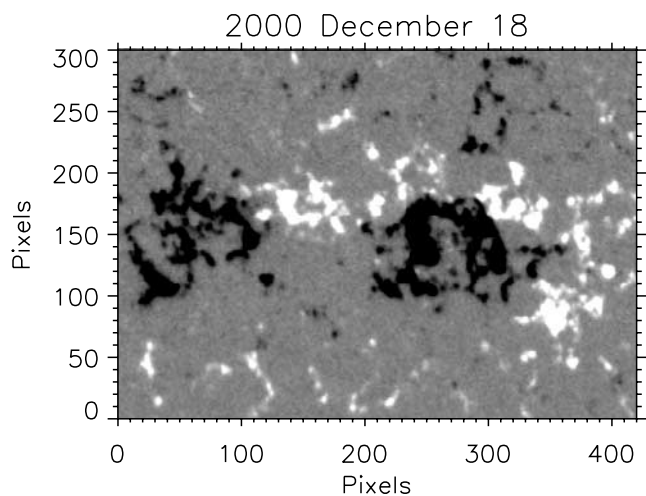
Figure 2. Example of magnetogram which is weak in field strength is shown here. Active region AR9269 obtained on Dec 18, 2000.

Table 1. The Date and Time of CME Occurrence, AR Which may be Responsible for CME, Co-ordinates, Projected Speed, Estimated Total Magnetic Energy and Class of Flare Respectively are Summarized Here

Date	Time (UT)	AR	Location	Speed (km s^{-1})	Magnetic potential energy (ergs)	X-ray class
May 01, 1998	23:40	AR8210	S18W05	585	4.86×10^{32}	M1.2
Nov 04, 1998	04:54	AR8375	N17W01	527	4.68×10^{32}	C5.2
Jun 08, 1999	21:50	AR8574	N30E03	726	5.86×10^{32}	C2.6
Jun 26, 1999	07:31	AR8598	N25E00	558	1.32×10^{33}	C7.0
Jun 29, 1999	07:31	AR8602	N18E07	634	$4.16 \times 10^{\wedge}32$	C3.0
Jun 29, 1999	18:54	AR8603	S14E01	438	6.47×10^{32}	C3.0
Jun 30, 1999	11:54	AR8603	S15E00	627	6.64×10^{32}	M1.9
Jul 28, 1999	05:30	AR8649	S15E00	457	4.49×10^{31}	
Jul 28, 1999	09:06	AR8649	S15E04	456	4.49×10^{31}	
Feb 10, 2000	02:30	AR8858	N27E01	944	1.57×10^{32}	C7.3
Apr 10, 2000	00:30	AR8948	S14W01	409	2.85×10^{32}	C8.1
Jun 07, 2000	16:30	AR9026	N20E02	842	6.47×10^{32}	X1.2
Jul 14, 2000	10:54	AR9077	N22E07	1674	7.01×10^{32}	X5.7
Jul 25, 2000	03:30	AR9097	N06W08	528	7.84×10^{32}	M8.0
Aug 09, 2000	16:30	AR9114	N11W09	702	4.38×10^{32}	C2.3
Sep 15, 2000	15:26	AR9165	N14E02	481	3.91×10^{32}	M2.0
Sep 15, 2000	21:50	AR9165	N14E01	257	3.83×10^{32}	C7.4
Sep 16, 2000	05:26	AR9165	N14W07	1215	3.96×10^{32}	M5.9
Oct 02, 2000	03:50	AR9176	S08E05	525	9.28×10^{32}	C4.1
Oct 02, 2000	20:26	AR9176	S08E05	569	8.34×10^{32}	C8.4
Nov 24, 2000	05:30	AR9236	N22W02	994	1.02×10^{33}	X2.0
Nov 24, 2000	15:30	AR9236	N22W07	1245	1.11×10^{33}	X2.3
Dec 18, 2000	11:50	AR9269	N14E03	510	1.16×10^{32}	C7.0
Apr 06, 2001	19:30	AR9415	S21E31	1270	9.01×10^{32}	X5.6
Apr 09, 2001	15:54	AR9415	S21W04	1192	8.11×10^{32}	M7.9
Apr 10, 2001	05:30	AR9415	S23W09	2411	8.28×10^{32}	X2.3
Apr 11, 2001	13:31	AR9415	S22W27	1103	8.26×10^{32}	M2.3
Apr 12, 2001	10:31	AR9145	S19W43	1184	8.51×10^{32}	X2.0
Apr 26, 2001	12:30	AR9433	N17W31	1006	1.88×10^{33}	M7.8
Oct 09, 2001	11:54	AR9653	S28E08	943	4.14×10^{32}	M1.4
Oct 22, 2001	15:06	AR9672	S21E18	1336	5.79×10^{32}	M6.7
Oct 25, 2001	15:26	AR9672	S16W21	1092	9.78×10^{32}	X1.3
May 16, 2002	00:50	AR9948	S20E14	600	6.80×10^{32}	C3.5
Jul 15, 2002	20:30	AR0030	N19W01	1132	1.76×10^{33}	X3.0
Jul 18, 2002	08:06	AR0030	N20W30	1111	2.14×10^{33}	X1.8
Aug 16, 2002	12:30	AR0069	S14E20	1459	2.41×10^{33}	M5.2
Nov 09, 2002	13:31	AR0180	S12W29	1633	7.35×10^{32}	M4.6

only an assumption, but could be easily falsified, had the vector magnetograms been available. This line bears a relation

$$\log_{10} V = -12.4(\pm 1.9) + 0.48(\pm 0.06) \log_{10} E$$

Thus the maximum speed of a CME for a given energy is seen to be proportional to the square root of the energy.

3. Discussions and Conclusions

[10] In using the projected speed of the halo CMEs we have made the assumption that the actual propagating speed is a function of the projected speed ($V = KV_p$). Figure 6 in *Michalek et al.* [2003] show that the difference between the projected speed and the corrected speed is $\approx$20%. The results of *Berger and Lites* [2003] shows that MDI systematically measures lower flux densities than Advanced Stokes Polarimeter. MDI underestimates the flux densities in a linear manner for MDI pixel values below $\approx$1200 G by a factor of $\approx$1.45. For the flux densities higher than 1200 G the underestimation becomes nonlinear. Below 1200 G, our results will be shifted uniformly in the direction of the abscissae (since the energy is proportional to square of the flux density and we use $\log_{10}$(energy)) and above 1200 G, our results are affected by very small amount, since the

number of pixels contributing to high field values are very small. So, both the projection effect for the expansion velocity and the calibration of MDI magnetograms will not substantially affect our results.

[11] From Figure 3 it is clear that there is a fairly strong relationship between the total magnetic energy with the
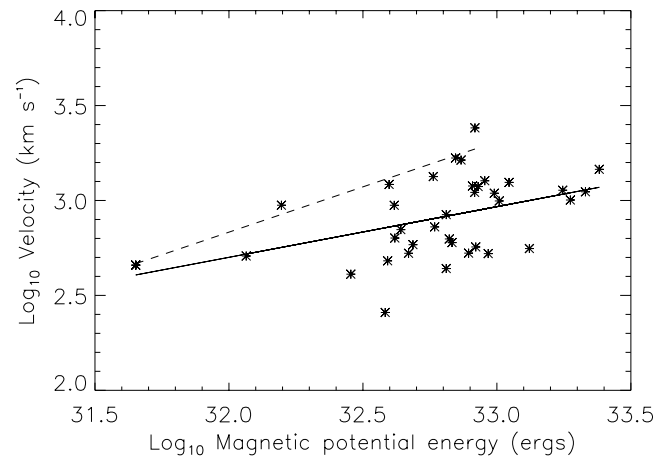
Figure 3. A plot of projected speed of CME vs magnetic potential energy of AR. The solid line corresponds to 0.26 slope and the dashed line corresponds to 0.48 slope.

projected speed of halo CME. The following physical conclusions can be drawn from the study. Although emerging flux in the core of an AR may be responsible for the occurrence of a CME [*Nitta and Hudson*, 2001], the maximum kinetic energy released in the CME seems to be well related to the total magnetic energy of the associated active region. This shows that for a large number of cases, it is an individual active region that powers a CME. In fact, the CME speed varies as 0.26th power of the magnetic energy in our study. Now, the shock speed in the classical Sedov solution for a blast wave varies as the 1/5th power of the injected energy for uniform density [*Choudhuri*, 1999]. Thus, the behavior of the solid line in Figure 3 is very close to the response of an homogeneous plasma to a sudden injection of energy. At the same time, the behavior of the dashed line in Figure 3 is closer to the response of a stratified plasma to a sudden injection of energy [*Sedov*, 1959].

[12] The idea that a CME is generated by a sudden injection of energy into the corona was explored by Dryer [cf. *Dryer*, 1974]. Those calculations were based on the response of the corona to a pressure pulse created by the sudden release of the energy in a flare. We call the injection sudden, whenever the time scale of energy input is shorter than the dynamical time scale of the system. The dynamical time scale is the time required for a pressure disturbance in the corona to traverse some typical distance, e.g., the pressure scale height. For a typical value of the sound speed in the corona of about 100 km s^{-1}, and the scale height of about 100000 km, we obtain a dynamical time of about 1000 sec. On the other hand, the energy release takes about a few minutes for a flare. Thus, the flare injects energy into the corona at a rate that is faster than the rate at which the coronal plasma can expand to smooth out the pressure enhancement. This was thought to result in a blast wave, as was borne out by the calculations. Later, it was seen that not all CMEs were related to flares [*Munro et al.*, 1979] and discrepancies in the chronology of flare on-set in relation to CME on-set [*Harrison*, 1995; *Zhang et al.*, 2001] were also noticed.

[13] However, recent observations have shown considerable dynamics in coronal active regions associated with CMEs [*Thompson et al.*, 1999]. Assuming that the coronal loops delineate magnetic field lines, the dynamics of these loops imply that CMEs are associated with re-arrangement of coronal magnetic field lines on the scale of active regions. Theoretically, the on-set of non-equilibrium in a quasi-static evolution of a coronal magnetic structure is known to result in a sudden expansion of a coronal loop to the nearest possible equilibrium state [*Low*, 1990]. This expansion of the magnetic field does imply the launch of a pressure pulse into the corona above the active region. The time scale for the injection of this mechanical energy would be the time required for the rearrangement of the field lines. This time would be the time required for an Alfven wave to traverse the active region. Assuming a conservative estimate of the magnetic field of 1G, and a density of 10^8 particles per cm^3, we get an Alfven speed of 200 km s^{-1}. This Alfven speed is also consistent with the observed speed of EIT waves. For a typical active region size of 30000 km, this leads to an Alfven time of 150 sec. Thus, the direct injection of mechanical energy via magnetic field expansion on a time scale which is small compared to the dynamical time scale of

the corona probably explains the resemblance of the empirical relationship seen in Figure 3 with the Sedov solution. As mentioned earlier, the range in speeds seen for a given value of magnetic energy could well be due to a range in the non-potentiality of the active region, a conjecture which can be easily falsified with vector magnetic data. It must also be understood that the empirical relationship of Figure 3 does not explain what produced the ejecta in the first place, but only provides a possible explanation of the driving mechanism for the ejecta. Classical blast waves do not carry ejecta, while a blast wave accompanied by ejecta has been called a quasi-blast [*Dryer*, 1974].

[14] We must remark here that we have confined our study to halo CMEs because of our need to provide an estimate of the initial CME speeds from the magnetic parameters of the associated AR. We are also constrained to look at ARs near central meridian passage to avoid severe projection effects in the calculation of the magnetic energy. The empirical relation of Figure 3, especially the dashed line allows us to make an estimate of the maximum possible speed of any CME that may result from an AR having a given magnetic energy. This ability would be very important for space weather predictions. Other parameters e.g., magnetic complexity, helicity etc. could also be studied. For the present, the magnetic energy seems to be a reasonable indicator for estimating the CME speed. In addition, the resemblance of the speed-energy relationship to the Sedov solution provides an exciting clue for understanding the driving mechanism for a CME.

References

Alissandrakis, C. E., On the computation of constant α force-free field, *Astron. Astrophys.*, *100*, 197, 1981.

Berger, T. E., and B. W. Lites, Weak-field magnetogram calibration using stokes polarimeter flux density maps-II. SOHO/MDI full-disk mode calibration, *Solar Phys.*, *213*, 213, 2003.

Brueckner, G. E., et al., The Large Angle Spectroscopic Coronagraph (LASCO), *Solar Phys.*, *162*, 357, 1995.

Chae, J., H. Wang, J. Qiu, P. R. Goode, L. Strous, and H. S. Yun, The formation of a prominence in active region NOAA 8688. I. SOHO/MDI observations of magnetic field evolution, *Astrophys. J.*, *560*, 476, 2001.

Chandrasekhar, S., *Hydrodynamic and Hydromagnetic Stability*, Oxford Univ. Press, 1961.

Choudhuri, A. R., *The physics of fluids and plasmas, An introduction to Astrophysics*, Cambridge University press, 118, 1999.

Delaboudiniere, J.-P., et al., Extreme Ultraviolet Imaging telescope for the SOHO mission, *Solar Phys.*, *162*, 291, 1995.

Dryer, M., Interplanetary shock waves generated by solar flares, *Space Sci Rev.*, *15*, 403, 1974.

Gopalswamy, N., Solar and geospace connections of energetic particle events, *Geophys. Res. Lett.*, *30*, 8013, 2003.

Harrison, R. A., The nature of solar flares associated with coronal mass ejection, *Astron. Astrophys.*, *304*, 585, 1995.

Howard, R. F., J. W. Harvey, and S. Forgach, Solar surface velocity fields detremines from small magnetic features, *Solar Phys.*, *130*, 295, 1990.

Low, B. C., Modeling Solar magnetic structures, *Measurements of solar vector magnetic fields*, *NASA conference publication 2374*, edited by M. J. Hagyard, 49, 1985.

Low, B. C., Equilibrium and dynamics of coronal magnetic fields, *Annu. Rev. Astron. Astrophys.*, *28*, 491, 1990.

Michalek, G., N. Gopalswamy, and S. Yashiro, A New method for estimating widths, velocities and source locations of halo coronal mass ejections, *Astrophys. J.*, *584*, 472, 2003.

Molodensky, M. M., Equilibrium and stability of force-free magnetic field, *Solar Phys.*, *39*, 393, 1974.

Munro, R. H., J. T. Gosling, E. Hildner, R. M. MacQueen, A. I. Poland, and C. L. Ross, The association of coronal mass ejection transients with other forms of solar activity, *Solar Phys.*, *61*, 201, 1979.

Nitta, N. V., and H. S. Hudson, Recurrent flare/CME events from an emerging flux region, *Geophys. Res. Lett.*, *28*(19), 3801, 2001.

Scherrer, P. H., et al., The Solar oscillations investigation—Michelson Doppler Imager, *Solar Phys.*, *162*, 129, 1995.

Sedov, L., *Similarity and Dimensional Methods in Mechanics*, Academic Press, 260, London/NY, 1959.

Srivastava, N., and P. Venkatakrishnan, Relationship between CME speed and Geomagnetic storm intensity, *Geophys. Res. Lett.*, *29*, 9, 2002.

Thompson, B. J., J. B. Gurman, W. M. Neupert, J. S. Newmark, J.-P. Delaboudiniere, O. C. St. Cyr, and S. Stezelberger, SOHO/EIT observations of the 1997 April 7 coronal tranient: Possible evidence of coronal moreton waves, *Astrophys. J.*, *517*, L151, 1999.

Yashiro, S., N. Gopalswamy, G. Michalek, N. Rich, C. O. St. Cyr, S. P. Plunckett, and R. A. Howard, *J. Geophys. Res.*, submitted, 2002.

Zhang, J., K. P. Dere, R. A. Howard, M. R. Kundu, and S. M. White, On the temopral relationship between coronal mass ejections and flares, *Astrophys. J.*, *559*, 452, 2001.

_____

P. Venkatakrishnan and B. Ravindra, Udaipur Solar Observatory, Physical Research Laboratory, P.O. Box 198, Dewali, Badi Road, Udaipur-313 001, Rajasthan, India. (bravindr@prl.ernet.in)